

# Radio Sources in Galaxy Clusters at 28.5 GHz.

Asantha R. Cooray<sup>1</sup>, Laura Grego<sup>1,2</sup>, William L. Holzapfel<sup>1,3</sup>, Marshall Joy<sup>4</sup>, John E. Carlstrom<sup>1,3</sup>

## ABSTRACT

We present serendipitous observations of radio sources at 28.5 GHz (1 cm), which resulted from our program to image thermal Sunyaev-Zeldovich (SZ) effect in 56 galaxy clusters. In a total area of  $\sim 0.8^\circ$  sq., we find 64 radio sources with fluxes down to  $\sim 0.4$  mJy ( $> 4\sigma$ ), and within  $250''$  from the pointing centers. The spectral indices ( $S \propto \nu^{-\alpha}$ ) of 54 sources with published low frequency flux densities range from  $-0.6 \lesssim \alpha \lesssim 2$  with a mean of  $0.77 \pm 0.06$ , and a median of 0.84. Extending low frequency surveys of radio sources towards galaxy clusters CL 0016+16, Abell 665, and Abell 2218 to 28.5 GHz, and selecting sources with  $S_{1.4\text{GHz}} \geq 7$  mJy to form an unbiased sample, we find a mean spectral index of  $0.71 \pm 0.08$  and a median of 0.71. We find 4 to 7 times more sources predicted from a low frequency survey in areas without galaxy clusters. This excess cannot be accounted for by gravitational lensing of a background radio population by cluster potentials, indicating most of the detected sources are associated with galaxy clusters. The differential source count slope,  $\gamma \sim 1.96$  ( $dN/dS \propto S^{-\gamma}$ ), is flatter than what is expected for a nonevolving Euclidean population ( $\gamma = 2.5$ ). For the cluster Abell 2218, the presence of unsubtracted radio sources with  $S_{28.5\text{GHz}} \leq 0.5$  mJy ( $\sim 5\sigma$ ), can only contribute to temperature fluctuations at a level of  $\Delta T \sim 10$  to  $25 \mu\text{K}$ . The corresponding error due to radio point source contamination in the Hubble constant derived through a combined analysis of 28.5 GHz SZ images and X-ray emission observations ranges from 1% to 6%.

*Subject headings:* galaxies: clusters: general — radio continuum — surveys — techniques: interferometric

## 1. Introduction

At present, much attention is focused on galaxy clusters due to the potential application of the thermal Sunyaev-Zeldovich (SZ) effect as a cosmological tool. Together with observations

---

<sup>1</sup>Department of Astronomy and Astrophysics, University of Chicago, Chicago IL 60637.

<sup>2</sup>Division of Mathematics, Physics, and Astronomy, California Institute of Technology, Pasadena, CA 91125.

<sup>3</sup>Enrico Fermi Institute, University of Chicago, Chicago IL 60637.

<sup>4</sup>Space Science Laboratory, NASA Marshall Space Flight Center, Huntsville AL 35812.

of X-ray emission, a measurement of the Hubble constant can be made if a complete sample of galaxy clusters is used (see reviews by Rephaeli 1995 and Birkinshaw 1998). Recent advances in interferometric tools have now allowed accurate mapping of the SZ decrement, producing two dimensional images which facilitate comparison of the X-ray emission and SZ effect. The SZ effect is typically of arcminute scale, which is not observable with most interferometers designed to achieve high angular resolution. The exception is the Ryle Telescope which has been used successfully to image the SZ effect at 2 cm. Another way to achieve the necessary beam size and sensitivity is to use an interferometer designed for millimeter wavelengths equipped with low-noise centimeter-wave receivers. We used this approach at the Owens Valley Radio Observatory Millimeter Array (OVRO) and Berkeley-Illinois-Maryland Association Millimeter Array (BIMA), where we have now detected the SZ effect in over 20 clusters at 1 cm, with preliminary results given in Carlstrom *et al.* (1996, 1997).

The accuracy of cm-wave observations of the SZ effect can be limited by emission from unresolved radio point sources towards galaxy clusters. The observing frequency of 28.5 GHz was influenced four different factors: the large beam size required to be sensitive to the SZ decrement using existing interferometers, the availability of low-noise HEMT amplifiers, atmospheric transparency, and the expected low radio source contamination due to falling flux density of most radio sources with increase in frequency. The interferometric technique makes it possible to detect radio point sources with longer baselines, which have little sensitivity to the SZ effect, and then remove their contribution from the short baseline data. Though such removal will produce point source-free SZ images, the uncertainties in removal of sources, due to the limited signal-to-noise and imperfect coherence, can introduce systematic noise. When the flux density of point sources are high, modeling and removal can result in systematic bias levels comparable to the size of the SZ effect. Since there are no published surveys at 28.5 GHz, it is not possible for us to predict accurately the number of radio sources expected to be present in a given cluster. In a few hours, however, it is possible for us to map a cluster with sufficient sensitivity to image unresolved 28.5 GHz radio sources which may complicate SZ mapping. Clusters with no bright sources, are then observed for longer periods,  $\sim 20$  to 50 hours, to obtain adequate signal-to-noise images of the SZ effect.

In this paper, our primary goal is to provide information on clusters which contain radio point sources at 28.5 GHz. Future publications will present our results on SZ detections in detail. Given that the cluster sample presented in this paper is incomplete in terms of either redshift or X-ray luminosity, statistical studies with this sample relating to cluster properties should be treated with caution. Section 2 of this paper describes observations made with OVRO and BIMA arrays. The detected 1 cm radio source sample and its properties are presented in Section 3, where we also estimate the radio source contamination in measuring the Hubble constant through a joint analysis of SZ and X-ray data by considering galaxy cluster Abell 2218 as an example.

## 2. Observations

The observed cluster sample is presented in Table 1. The pointing centers of clusters were derived from existing literature and were checked with optical images when such images were available. Usually, optical coordinates of the central galaxy were taken as the pointing coordinates of a given cluster. If there was not a clear central galaxy, centroid coordinates from X-ray observations were used (e.g., Ebeling *et al.* 1996, Ebeling *et al.* 1997). Our sample ranges in redshift from  $\sim 0.15$  to  $0.85$ , with the lower limit imposed by the large angular scale of nearby clusters to which the interferometer would not be sensitive, and the upper limit based on the X-ray detection limit of distant clusters. This sample was observed at OVRO with six telescopes of the millimeter array during summers of 1995 and 1996, with six telescopes of the BIMA array during summer of 1996, and with nine telescopes of the BIMA array during summer of 1997.

We equipped both arrays with low-noise 1 cm receivers, especially designed for the detection of SZ effect. Each receiver contains a cryogenically cooled scalar feed-horn and HEMT amplifier covering the frequency range 26 to 36 GHz. The system temperatures scaled above the atmosphere ranged from 30 to 45 K. During the 1995 OVRO observations, our receivers were sensitive to linear polarization. Due to the rotation of polarized intensity across the sky of our calibrating sources, which are expected to be polarized up to 10%, the calibration process for cluster fields observed in 1995 introduced additional uncertainties. For long time series calibrator observations with large parallactic angle coverage, the flux variation can be corrected by estimating the polarization. However, for short observations we expect an additional 5% to 10% uncertainty in the flux density of sources imaged in our 1995 cluster sample. We upgraded our receivers so that observations during 1996 and 1997 detected circular polarization, which is not subject to this effect. For clusters that were initially observed in 1995 and were reobserved in later years, we have opted to use latest data to avoid additional uncertainties.

Integration time on each cluster field ranged from  $\sim 3$  hours to 50 hours, with the short integration times on clusters where we happened to detect a bright radio source. For each cluster,  $\sim 5$  minute observations of a secondary calibrator from the VLA calibrator list were interleaved with every  $\sim 25$  minutes spent on a cluster. Between different clusters,  $\sim 45$  to 60 minutes were spent observing planets, with care taking to observe Mars frequently since it is used as our primary flux calibrator. The flux densities of the secondary gain and phase calibrators were calibrated relative to Mars. The brightness temperature of Mars was calculated using a thermal-radiative model with an estimated uncertainty of 4% (Rudy 1987). In Table 2, we present 1 cm flux densities of gain and phase calibrators determined through this process for the summer 1997 observations, which can be useful for future observational programs at this wavelength. Some of these calibrator sources are likely to be variable at 28.5 GHz, but during the time scale of our 1997 observations, 2 months, the maximum variation was found to be less than 4%. The uncertainties in the reported flux densities in Table 2 are less than  $\sim 5\%$ .

For the OVRO data, the MMA software package (Scoville *et al.* 1993) was used to calibrate

the visibility data and then write it in UV-FITS format. We flagged all of the data taken when one antenna was shadowed by another, cluster data that was not bracketed in time by phase calibrator data (mostly at the end or beginning of an observation), and, rarely, data with anomalous correlations. We followed the same procedure for data from BIMA, except that MIRIAD software package (Wright & Sault 1993) was used for calibration and data editing purposes. The image processing and CLEANing were done using DIFMAP (Shepherd, Pearson, & Taylor 1994). We cleaned all fields uniformly, based on the rms noise level. Our automated mapping algorithm within DIFMAP was able to find sources with extended structures, which when compared with low frequency data, such as VLA D-Array 1.4 GHz NVSS survey (Condon *et al.* 1996), were confirmed for all cases. In general,  $\sim 2000$  clean iterations with a low clean loop gain of 0.01 was chosen to avoid instabilities and artifacts that can occur in fields with a large number of sources.

We looked for radio point sources in naturally weighted maps with visibilities greater than 1 k $\lambda$  in BIMA data and 1.5 k $\lambda$  in OVRO data. Since the interferometer is less sensitive with only the long baseline data, we obtained flux densities of detected sources in maps made with all visibilities. Using images made with all the UV data also allowed us to look for sources with extended structure. Typical synthesized beam sizes in these images range from 12'' to 30''. For typical cluster and control blank fields with no bright radio sources ( $\geq 1$  mJy), and no evident SZ decrement, the noise distribution was found to be a Gaussian centered at zero. These images did not contain any pixels with peak flux density  $\leq -4 \sigma$  within 250''. The mean rms noise level for all our 56 cluster observations is 0.24 mJy beam $^{-1}$ , while the lowest rms noise level is 0.11 mJy beam $^{-1}$  for BIMA observations and 0.07 mJy beam $^{-1}$  for OVRO observations. Given the decrease in sensitivity due to the primary beam attenuation from the image centers, we only report sources within 250'' of the pointed coordinates. A Gaussian-noise analysis suggested that within 250'' from the center in all 56 cluster fields, only 1 noise pixel is expected at a level above  $4 \sigma$ . Among all 56 cluster fields, there was only one instance where a source was clearly detected at a distance greater than 250'' from the cluster center; In CL 0016+16 we found a source  $\sim 290''$  away from the pointed coordinates, which is discussed in Carlstrom *et al.* (1996).

### 3. Results and Discussion

In Table 3, we report the flux densities of detected 1 cm radio sources. When calculating these flux densities, we have corrected for the beam response. To determine the primary beam pattern at BIMA, the radio source 3C454.3 with a flux density of  $\sim 8.7$  Jy at 28.5 GHz was observed with a grid pattern of pointing offsets, and then a two dimensional Gaussian fit was performed to the flux density values. A 300'' by 300'' grid with 75'' spacing was best fit by a Gaussian with a major axis of 386'', a minor axis of 380'' (FWHM) and a position angle  $-85.31^\circ$ , with an uncertainty of 3''. The rms residual from the fit was  $\sim 0.01$  Jy. A 360'' by 360'' grid with 90'' spacing was best fit by a Gaussian with a major axis of 382'' and a minor axis of 379'', also with rms residual of 0.01 Jy. Given the small difference between two axes and positional uncertainty of at least  $\sim 5''$  at BIMA,

we have utilized a symmetrical Gaussian model with a  $380''$  FWHM half-power point. At OVRO, we have made holographic measurements of the beam pattern and have corrected the fluxes based on the position of sources relative to a modeled Gaussian distribution, which resulted in a primary beam of  $235''$  (FWHM).

For our 1 cm sample, we searched literature for low frequency counterparts within  $15''$  from the 28.5 GHz radio source coordinates. A low frequency source was accepted as a counterpart when the difference between our coordinates and published coordinates was less than the astrometric uncertainty in our coordinates and the low frequency counterpart coordinates. The error in 1 cm coordinates ranges from  $\sim 3''$  to  $10''$ , which is equivalent to the image resolution divided by the signal-to-noise with which the source was detected. For cluster fields with bright radio sources, the signal-to-noise was low due to small integration times, producing uncertainties in position as high as  $\sim 10''$ . Still, identification of such sources was easier due to their relatively high flux densities. For published sources, the astrometric errors ranged from sub-arcseconds, mostly from VLA observations, to few arcseconds. The mean difference between our coordinates and published coordinates was  $\sim 6''$ . Based on Moffet & Birkinshaw (1989), we estimated the field density of 5 GHz radio sources towards clusters with a flux limit of 1 mJy is  $\sim 25 \text{ degree}^{-2}$ . Therefore, the probability of an unrelated radio source, with a 5 GHz flux density above 1 mJy, lying within  $6''$  is  $< 0.5\%$ .

When there is a well known counterpart from literature coincident with the detected 1 cm source, we have noted the commonly used name in Table 3. We have calculated the spectral index of individual radio sources by fitting all known flux densities, with spectral index  $\alpha$  defined as  $S \sim \nu^{-\alpha}$ . In Fig. 1, we show a histogram of the calculated spectral indices of 52 sources for which we have found radio observations at other frequencies. In this plot, we have not included the sources 1635+6613 towards Abell 2218 and 1615-0608 towards Abell 2163, which are found with flux densities that peak between 1.4 GHz and 28.5 GHz (e.g., Fig. 2). These sources may indicate self-absorbed radio cores, with spectral turnover due to free-free absorption. Such turnovers in inverted spectra are found in Gigahertz Peaked Spectrum (GPS) sources, though definition of GPS sources calls for peaked spectra between 0.5 and 10 GHz (De Vries, Barthel, & O’Dea 1997). The increase in turnover frequency well above 10 GHz, could be due to an increase in ambient density. Also, 1615-0608 towards Abell 2163 is known to be variable based on VLA observations by Herbig & Birkinshaw (1994). During our observations, the flux density of this source did not change significantly: we measured a flux density of  $1.12 \pm 0.29$  mJy in 1995 (OVRO) and  $0.93 \pm 0.42$  mJy in 1997 (BIMA) at 1 cm. In Table 3, we report the 1995 flux density value since tabulated VLA measurements were made closer to our 1995 observations. Abell 2163 is also known to contain one of the largest radio halo sources ever found. We did not detect any emission from the cluster center, which is understandable given that the halo was detected only at 1.4 GHz, with an integrated flux density of  $\sim 6$  mJy and a steep spectral index of  $\sim 1.5$ .

In our sample we also find 3 sources with inverted spectra between 1.4 and 28.5 GHz: 0152+0102 towards Abell 267, 0952+5151 towards Zw 2701, and 1155+2326 towards Abell 1413. These could

either represent free-free emission due to starburst, or synchrotron emission from a weak AGN, or both, with an optically thick part of a thermal bremsstrahlung component that extends to high frequencies. Since the inverted spectral indices are less than -2, which is the value expected for optically thick thermal sources, it is more likely that these sources represent multiple non-thermal components. The relatively flat-spectrum ( $-0.5 \lesssim \alpha \lesssim 0.5$ ) sources may indicate unresolved cores and hotspots, and further high resolution observations are necessary to resolve full structure. These sources include 0152+0102 towards Abell 267 and 2201+2054 towards Abell 2409.

In Table 3, the identification of a source as a central galaxy (CG) was only made when we have used the optical coordinates of central galaxy from literature as the pointing coordinates, and when we have detected a radio source at 1 cm within  $10''$  of the observed coordinates. We have found 13 such sources, which may well represent the radio emission associated with central cD galaxy of the cluster.

Due to the low resolution of our observations, most of the radio sources are unresolved, but in a few cases we find some evidence for extended emission. These sources include 0037+0907 and 0307+0908 towards Abell 68 (Fig. 3), 1716+6708 (4C +67.26) towards RXJ1716+6708 (Fig. 4), 1335+4100 (4C +41.26) towards Abell 1763, and 1017+5934 towards Abell 959. The nature of extended emission associated with these sources should be further studied, and high resolution observations at several frequencies will be helpful in this regard. 1335+4100 (4C +41.26) towards Abell 1763 is a well studied FR II type radio source (e.g., Owen 1975).

For our sample of 52 radio sources with known flux densities at lower frequencies, a mean spectral index of  $0.77 \pm 0.06$ , and a median of 0.84 are found. If the three sources with inverted spectral indices are not considered, the mean and median rise to  $0.85 \pm 0.06$  and 0.85 respectively. To avoid a biased estimate for the spectral index distribution, however, we must consider counterparts at 1 cm for all sources detected at lower frequencies. Galaxy clusters CL 0016+16, Abell 2218 and Abell 665 have been observed at 1.4, 4.85, 14.9 and 20.3 GHz by Moffet & Birkinshaw (1989), and their observations are complete to a flux density limit of 1 mJy at 4.85 GHz. In each of these three clusters, we selected sources in the low frequency survey which were located within  $300''$  from the cluster center. We list these sources, their flux densities at 1.4 GHz, expected flux densities at 28.5 GHz based on 1.4 and 4.85 GHz spectral index, observed flux densities at 28.5 GHz, and calculated spectral indices between 1.4 and 28.5 GHz in Table 4. At 28.5 GHz, we detect all sources with flux densities greater than 7 mJy at 1.4 GHz, at a detection level greater than  $3\sigma$ . We looked for counterparts of these sources at 28.5 GHz, which should form a complete sample and not bias the spectral index distribution. Also, given that we looked for 28.5 GHz counterparts only within  $15''$  of the 1.4 GHz source coordinates, we expect all detections at a level above  $3\sigma$  to be real. For this sample, we find a mean spectral index of  $0.71 \pm 0.08$ , and a median of 0.71. The 1 cm spectral index distribution agrees with that of the 6 cm mJy population with a median of 0.75 (Donnelly *et al.* 1987). However, the 1 cm distribution is steeper than the sub-mJy and the  $\mu$ Jy populations, where medians of 0.35 (Windhorst *et al.* 1993) and 0.38 (Fomalont *et al.* 1991) were found at 4.85 and 8.4 GHz respectively. The latter sub-mJy populations have been identified with faint blue

galaxies. Our sample could be part of the lower frequency mJy and sub-mJy populations, but given the lack of detailed optical data for most of our sources, we cannot exactly state the optical nature of our 28.5 GHz sample.

We compare our results with a 1.4 GHz survey by Condon, Dickey, & Salpeter (1990) in areas without rich galaxy clusters, in order to address whether we are finding an overabundance of radio sources at 28.5 GHz towards galaxy clusters. They found a total of 354 radio sources, down to a flux limit of 1.5 mJy, in a total surveyed area of about 12 square degrees. Seven of these sources are thought to be associated with galaxy clusters, which includes Abell 851 (source 0942+4658 in Table 3). Ignoring this small contamination, we calculated the expected flux densities of the 1.4 GHz sources at 28.5 GHz based on the mean spectral index value of our sample. For a spectral index of 0.71, we found 170 sources with fluxes greater than 0.4 mJy at 1 cm, which is the lowest  $4\sigma$  detection limit of our observations. Given that the ratio of total area observed by the 1.4 GHz survey and our survey is  $\sim 15$ , we only expect  $\sim 7$  to 15 sources be present with flux densities greater than 0.4 mJy at 28.5 GHz, and therefore be detected in our observations. Given that we find 62 sources, ignoring the inverted and unusual spectrum sources, we conclude that we are finding at least  $\sim 4$  times more sources than usually expected. Given the primary beam attenuation and the nonuniformity of flux density limit from one cluster field to another, the above ratio is only a lower bound on the calculated ratio. If we take these facts into account, we find that our sample at 28.5 GHz contains 7 times more than one would normally expect based on a low frequency radio survey devoid of clusters. This result may have some consequences when planning and reducing data from large field observations, such as our planned degree-square SZ effect survey.

The reason that we are seeing more sources might be explained through gravitational lensing of a background radio population by cluster potentials. Our cluster sample ranges in redshift from  $\sim 0.15$  to 0.85, with a mean of  $0.29 \pm 0.02$ , and a median of 0.23. If the excess source counts are indeed an effect due to lensing, the background population should be at a lower flux level than what we have observed. An optimal lensing configuration suggests that background sources should be at angular diameter distances twice that of the galaxy clusters, which are assumed to be lensing potentials. For the range of cluster redshifts, the background source sample should be at redshifts between  $\sim 0.4$  and 1.4, with a mean redshift of  $\sim 0.7$ . In terms of well known radio source samples, a possibility of such an unlensed population between redshifts of 0.4 and 1.4 is the sub-mJy radio sources at 5 and 8.4 GHz (Windhorst *et al.* 1993). For simplicity, we consider a cluster potential based on the singular isothermal sphere (SIS) model of Schneider, Ehlers & Falco (1992). Such a potential brightens, but dilutes the spatial distribution, background sources by the magnification factor,

$$\mu(\theta) = \left| 1 - \frac{\theta_E}{\theta} \right|^{-1}, \quad (1)$$

where  $\theta$  is the angle, or distance, to radio source from cluster center, and  $\theta_E$  is the Einstein angle, which depends on the distances to a given cluster and background radio sources ( $\theta > \theta_E$ ). The Einstein angle can be observationally determined through optical images of clusters where background sources are lensed into arcs and whose redshift is known. In order to estimate reliable

Einstein angles for background sources at redshifts around  $\sim 0.7$ , we considered two well studied clusters. In Abell 2218 an arc is found  $\sim 21''$  from the cluster center with a measured redshift of 0.702 (Pelló *et al.* 1992), and in Abell 370 an arc is found  $\sim 36''$ , with a redshift of 0.72 (Kneib *et al.* 1994). The 1 cm source sample ranges from  $\sim 0$  to  $250''$  in distance from individual cluster centers, with a mean of  $\sim 94 \pm 10''$ , and a median of  $97''$ . These values suggest a mean magnification factor of  $\sim 1.4$ , suggesting that we should expect 10 to 20 sources at 28.5 GHz towards galaxy clusters, based on our earlier estimate of 7 to 15 sources and not accounting for the spatial dilution due to lensing. It is unlikely that lensing can account for the significant excess number of radio sources we have detected at 28.5 GHz. Also, VLA A-array observations at 1.4 GHz to a flux density limit of 1 mJy have not yet produced convincing evidence for the existence of gravitationally lensed radio sources, such as radio arcs, towards galaxy clusters (e.g. Andernach *et al.* 1997). An apparent detection of gravitational lensing towards clusters, based on the tangential orientation of radio sources, is discussed in Bagchi & Kapahi (1995). Recently, Smail *et al.* (1997) have observed an increase in sub-mm surface flux density towards clusters Abell 370 and CL 2244-02, which was interpreted as due to the gravitational lensing by cluster potentials of strongly star-forming galaxies at redshifts  $\gtrsim 1$ . Given that the number counts of our sample cannot be totally explained as due to a lensing effect and that we do not have enough resolution to look for alterations that might be a result of lensing situations, we conclude that a large fraction of the detected 1 cm sample must be associated with clusters towards which they were found.

In Fig. 6, we plot the source counts per solid angle at 1 cm, which were binned in logarithmic intervals of 0.2 mJy into 8 different bins. The solid angle for each flux bin takes into account the variation in sensitivity of our observations. A large number of sources are found in the lowest bin, which may have a nonuniform detections due to the variation in noise level from one cluster field to another. The maximum-likelihood fit to a power-law distribution of the observed sources, and normalised to the source counts greater than 1.6 mJy, is  $N(> S) = (59^{+20}_{-15}) \times (S/\text{mJy})^{-0.96 \pm 0.14}$  in a total surveyed area of  $2.5 \times 10^{-4}$  sr, where  $N(> S)$  is an integral representation of number of sources with flux densities greater than  $S$  in mJy. Given that we only looked for sources towards a sample of X-ray luminosity selected galaxy clusters, and that we have not carried out 28.5 GHz observations to a uniform flux density limit in all observed fields, the above number count-flux relationship should not be treated as true in general for all radio sources at 28.5 GHz. However, our result may be useful when studying radio source contamination in planned CMB anisotropy and SZ experiments. The corresponding differential source count slope  $\gamma$  is  $\sim 1.96$  ( $dN/dS \propto S^{-\gamma}$ ). This slope is similar to what is found for 6 cm mJy radio sources ( $\gamma \approx 1.8$ , Donnelly *et al.* 1987) with similar flux densities as our sample, but is marginally flatter than sub-mJy population of radio sources ( $\gamma \approx 2.3$ , Windhorst *et al.* 1993). The flattening of the slope from the expected Euclidean value ( $\gamma = 2.5$ ) is likely to be due to the dependence of radio luminosity with galaxy cluster properties, as we may be finding bright radio sources towards X-ray luminous clusters.

Recently, Loeb & Refregier (1997) have suggested that the value of the Hubble constant determined through a joint analysis of SZ and X-ray data may be underestimated due to radio point

source contamination. We address this issue based on our 28.5 GHz data and low frequency observations towards Abell 2218, which was also studied in Loeb & Refregier (1997). There are 5 known sources within  $300''$  from the cluster center (Moffet & Birkinshaw 1989), out of which we detect 3 (see Fig. 5) down to a flux density of  $\sim 1$  mJy. By subtracting these three sources and using all visibilities and a Gaussian UV taper of 0.5 at  $0.9$  k $\lambda$ , we find a SZ decrement with a signal-to-noise ratio greater than 20. The restored beam size of this map is  $110''$  by  $98''$ . By extrapolating low frequency flux densities to  $1$  cm, based on the  $1.4$  and  $4.85$  GHz spectral indices, we infer an unaccounted intensity of  $\sim 250$  Jy sr $^{-1}$ . Assuming that the flux densities in the map at the expected location of the unsubtracted sources are the real  $28.5$  GHz flux densities of the undetected sources, we estimate an upper limit on the unaccounted intensity of  $\sim 590$  Jy sr $^{-1}$ . The latter value is equivalent to the noise contribution in the observed SZ decrement. The two intensities are equivalent to  $\sim 10$  and  $25$   $\mu$ K respectively, which we take as the range of errors in the observed SZ temperature decrement  $\Delta T_{sz}$ . The central temperature fluctuation due to SZ decrement towards Abell 2218,  $\Delta T_{sz}$  ranges from  $\sim 0.6$  to  $1.1$  mK, based on different  $\beta$ -models to SZ morphology (see also Jones *et al.* 1993). The Hubble constant,  $H$ , varies as  $H \propto T_{sz}^{-2}$ . Thus, the offset in true and calculated Hubble constant,  $\Delta H$ , is:

$$\frac{\Delta H}{H} \sim \frac{2\Delta T_{sz}}{T_{sz}}. \quad (2)$$

For Abell 2218, we find that the fractional correction to the Hubble constant from not accounting for sources with flux densities less than  $0.5$  mJy at  $28.5$  GHz ranges from  $\sim 1\%$  to  $6\%$ . If sources with flux densities less than  $0.1$  mJy are not accounted for, we estimate an upper limit on the offset of  $2\%$ . These values are in agreement with Loeb & Refregier (1997), who suggested that the  $5$  GHz sub-mJy population (Windhorst *et al.* 1993) may affect the derivation of the Hubble constant at  $15$  GHz by  $7\%$  to  $13\%$ , if sources less than  $0.1$  mJy at  $15$  GHz not properly taking into account. Given that the intensity of the SZ decrement has a spectral index of  $-2$ , and assuming a spectral index of  $0.7$  for the radio source flux contribution, we estimate the frequency dependence of the correction as  $\nu^{-2.7}$ . Thus, at  $15$  GHz, we also find that the Hubble constant may be underestimated up to  $13\%$ . The contribution from free-free emission, which scales as  $\nu^{-0.1}$ , is not expected to contribute to underestimation of the Hubble constant at a level more than  $0.1\%$  at  $28.5$  GHz. At high frequencies ( $> 90$  GHz), the free-free and dust emissions, with dust scaling as  $\nu^\beta$ ,  $3 < \beta < 4$  at  $100$  GHz, may become the dominant source of error. Therefore, based on the  $28.5$  GHz data towards Abell 2218, we conclude that the error in the Hubble constant through a joint analysis of SZ data at  $28.5$  GHz and X-ray emission observations is not expected to be larger than the error introduced by the analysis (such as  $\beta$ -models) and unknown nature of the galaxy cluster shape (oblate vs. prolate etc.), which can amount up to  $30\%$  (e.g. Roettiger *et al.* 1997).

We wish to thank the staff at OVRO and BIMA observatories for their assistance with our observations, in particular J. R. Forster, J. Lugten, S. Padin, R. Plambeck, S. Scott, and D. Woody. We also thank C. Bankston and P. Whitehouse at the MSFC for helping with the construction of the SZ receivers, and M. Pospieszalski for the Ka-band HEMT amplifiers. We also gratefully

acknowledge H. Ebeling, A. Edge, H. Bohringer, S. Allen, C. Crawford, A. Fabian, W. Voges, J. Huchra and P. Henry for providing us results from X-ray observations of galaxy clusters prior to publication. ARC acknowledges useful discussions with A. Fletcher on an early draft of the paper. JEC acknowledges support from a NSF-Young Investigator Award and the David and Lucile Packard Foundation. Initial support to build hardware for the SZ observations came from a NASA CDDF grant. Radio astronomy with the OVRO millimeter array is supported by the NSF grant AST96-13717, and astronomy with the BIMA array is supported by the NSF grant AST96-13998.

## REFERENCES

- Andernach, H., Gubarov, A. G., Slee, O. B. 1997, *Proc. of Observational Cosmology with the new Radio Surveys*, eds. M. Bremer, N. Jackson & I. Perez-Fournon, Kluwer Acad. Press.
- Bagchi, J., Kapahi, V. K. 1995, *JApA*, 16, 131.
- Becker, R. H., White, R. L., Edwards, A. L. 1991, *ApJS*, 75, 1.
- Becker, R. H., White, R. L., Helfand, D. J. 1995, *ApJ*, 450, 559.
- Birkinshaw, M. 1998, submitted to *Physics Reports*.
- Carlstrom, J. E., Grego, L., Joy, M. 1996, *ApJ*, 456, 75.
- Carlstrom, J. E., Grego, L., Holzapfel, W. L., Joy, M. 1997, *Proc. of the 1996 Texas Relativistic Astrophysics Symp.*, ed. A. Olinto, in press.
- Condon, J. J., Dickey, J. M., Salpeter, E. E. 1990, *AJ*, 99, 1071.
- Condon, J. J., Cotton, W. D., Greisen, E. W., Yin, Q. F., Perley, P. A., Taylor, G. B., Broderick, J. J. 1996, in preparation.
- De Vries, W. H., Barthel, P. D., O’Dea, C. P. O. 1997, *A&A*, 321, 105.
- Donnelly, R. H., Partridge, R. B., Windhorst, R. A. 1987, *ApJ*, 321, 94.
- Douglas, J. N., Bas, F. N., Bozayan, F. A., Torrence, G. W., Wolfe, C. 1996, *AJ*, 111, 1945.
- Ebeling, H., Voges, W., Bohringer, H., Edge, A. C., Huchra, J. P., Briel, U. G., 1996, *MNRAS*, 281, 799 (see also erratum, *MNRAS* 283, 1103).
- Ebeling, H., et al. 1997, *MNRAS*, submitted.
- Ficarra, A., Grueff, G., Tomassetti, G. 1985, *A&AS*, 59, 255.
- Fomalont, E. B., Windhorst, R. A., Kristain, J. A., Kellerman, K. I. 1991, *AJ*, 102, 1258.

- Grainge, K., Jones, M., Pooley, G., Saunders, R., Baker, J., Haynes, T., Edge, A. 1996, MNRAS, 278, 17.
- Gregory, P. C., Condon, J. J. 1991, ApJS, 75, 1011.
- Griffith, M. R., Wright, A. E., Burke, B. F., Ekers, R. D. 1995, ApJS, 97, 347.
- Gioia, I. M., Luppino, G. A. 1994, ApJS, 94, 583.
- Henry, J. P., Gioia, I. M., Mullis, C. R., Clowe, D. I., Luppino, G. A., Boehringer, H., Briel, U. G., Voges, W., Huchra, J. P. 1997, AJ, 114, 1293.
- Herbig, T., Birkinshaw, M. 1994, BAAS, 26, 1403.
- Jones, M., Saunders, R., Alexander, P., Birkinshaw, M., Dilon, N., Grainge, K., Hancock, S., Lasenby, A., Lefebvre, D., Pooley, G. 1993, Nature, 365, 320.
- Kneib, J. P., Mathez, G., Fort, B., Mellier, Y., Soucail, G., Longaretti, P. Y. 1994, A&A, 286, 701.
- Loeb, A., Refregier, A. 1997, ApJ, 476, 59.
- Moffet, A. T., Birkinshaw, M. 1989, AJ, 98, 1148.
- Owen, F. N. 1975, AJ, 80, 263.
- Pelló, R., Le Borgne, J. F., Sanahuja, B., Mathez, G., Fort, B. 1992, A&A, 266, 6.
- Rephaeli, Y. 1995, ARA&A, 33, 541.
- Robertson, J. G., Roach, J. 1990, MNRAS, 247, 387.
- Roettiger, K., Stone, J. M., Mushotzky, R. F. 1997, ApJ, 482, 588.
- Rudy, D. J. 1987, Ph.D. thesis, California Institute of Technology.
- Schneider, P., Ehlers, J., Falco, E. E. 1992, Gravitational Lenses (New York: Springer).
- Scoville, N. Z., Carlstrom, J. E., Chandler, C. J., Phillips, J. A., Scott, S. L., Tilanus, R. P. J., Wang, Z. 1993, PASP, 105, 1482.
- Shepherd, M. C., Pearson, T. J., Taylor, G. B. 1994, BAAS, 26, 987.
- Slee, O. B., Roy, A. L., Savage, A. 1994, Australian Journal of Physics, 47, 145.
- Smail, I., Ivison, R. J., Blain, A. W. 1997, ApJ, in press (also astro-ph/9708135).
- White, R. L., Becker, R. H. 1992, ApJS, 79, 331.
- Windhorst, R. A., Fomalont, E. B., Partridge, R. B., Lowenthal, J. D. 1993, ApJ, 405, 498.

Wright, M. C. H., Sault, R. J. 1993, ApJ, 402, 546.

Fig. 1.— Spectral-index distribution of 52 sources with  $S > 0.4$  mJy at 28.5 GHz based on flux densities at lower frequencies (see Table 3).

Fig. 2.— Radio spectrum of 1635+6619 towards Abell 2218 (source 12 of Moffet & Birkinshaw 1989), showing the turnover of inverted spectrum between 20.3 and 28.5 GHz.

Fig. 3.— 28.5 GHz map of A68 showing an extended source, 0037+0907 north peak and 0307+0908 south peak, with structure that corresponds with the 1.4 GHz NVSS D-Array observations of the same cluster. The 28.5 GHz contours are at steps of 0.4 mJy ( $2.5 \sigma$ ) and shown in false color scale is the VLA D-Array NVSS 1.4 GHz map.

Fig. 4.— 28.5 GHz map of 1716+6711 (4C +67.26) towards RXJ1716+6708 ( $z = 0.813$ , Henry *et al.* 1997), where we detect the source with a total flux density of 10.41 mJy and with a beam size of  $24.1$  by  $17.8''$  (FWHM) at  $89.8^\circ$ . The extended structure of the source is clearly seen. The 28.5 GHz contours are at 1.20 mJy ( $2 \sigma$ ).

Fig. 5.— 28.5 GHz total intensity contour map of Abell 2218 which have been plotted on to 1.4 GHz VLA D-Array NVSS observations of the same cluster. At 28.5 GHz, we detect 3 sources at a noise level greater than  $4 \sigma$ . Source 1635+6619 has an unusual spectrum that peaks between 1.4 and 28.5 GHz (Fig. 2). The 28.5 GHz contours are at 0.23 mJy ( $2 \sigma$ ), with false color scale VLA D-Array NVSS 1.4 GHz map.

Fig. 6.— The source counts at 28.5 GHz, binned in logarithmic intervals of 0.2 mJy. These counts are fitted best with a power-law distribution with an exponent  $\sim -0.96 \pm 0.14$ . The corresponding differential source count slope  $\gamma$  ( $dN/dS \propto S^{-\gamma}$ ) is  $\sim 1.96$ .

Fig. 7.— Radio sources towards Abell 520, with 28.5 GHz BIMA 1997 total intensity contours overlaid on the 1.4 GHz VLA D-Array NVSS survey map. The 28.5 GHz contours are at 0.21 mJy ( $1 \sigma$ ), while the VLA D-Array NVSS 1.4 GHz map is represented with false color.

Fig. 8.— Radio sources towards Abell 1576, with OVRO 1996 total intensity contours overlaid on the VLA D-Array NVSS 1.4 GHz map. The Double lobe source to the west is 8C 1234+634. We only detect emission from its northern lobe, but this may be due to the rapid fall off of the OVRO primary beam at these distances from the cluster center. The 28.5 GHz contours are at 0.22 mJy ( $1 \sigma$ ), and the 1.4 GHz map is shown in false color.

TABLE 1. Cluster Sample

Cluster Name	RA (J2000.0)	Dec (J2000.0)	Redshift	Obs. Location	$S_{rms}$
CL0016+16	00 18 34.633	16 26 18.32	0.54	HC96,HC97	0.16,0.15
Abell 68	00 37 06.654	09 09 18.85	0.255	HC97	0.42
Abell 267	01 52 41.936	01 00 24.12	0.23	HC97	0.51
Abell 348	02 23 58.978	-08 35 39.43	0.27	OV96	0.30
Abell 370	02 39 52.501	-01 34 20.00	0.374	HC97	0.21
Abell 383	02 48 03.584	-03 32 04.42	0.187	HC97	0.24
MS0302.7+1658	03 05 31.714	17 10 02.78	0.423	OV95	0.20
RXJ0439+07	04 39 01.191	07 15 36.10	0.23	HC97	0.20
Abell 520	04 54 12.654	02 55 24.00	0.203	HC97	0.33
MS0451.6-0305	04 54 10.828	-03 00 56.82	0.55	OV96	0.13
Abell 586	07 32 20.321	31 38 01.86	0.171	HC96	0.22
Abell 611	08 00 56.745	36 03 21.58	0.288	OV95	0.13
Abell 665	08 38 49.652	65 49 42.42	0.182	HC96,HC97	0.14,0.17
Abell 697	08 24 57.563	36 21 59.34	0.282	OV95	0.28
Zw 1953	08 50 10.096	36 05 09.38	0.32	HC97	0.20
Zw 2089	09 00 37.921	21 54 57.39	0.23	HC97	0.28
Abell 781	09 20 28.798	30 31 08.18	0.298	HC97	0.24
Abell 851	09 42 56.631	49 59 20.19	0.402	HC97	0.18
Zw 2701	09 52 47.509	51 53 27.36	0.214	HC97	0.23
Abell 959	10 17 35.890	59 34 05.62	0.35	OV96	0.11
Abell 990	10 23 41.828	49 08 38.23	0.144	HC96	0.19
Abell 992	10 22 33.950	20 29 29.82	0.247	OV96	0.16
Zw 3146	10 23 39.730	04 11 10.85	0.29	OV96	0.22
MS1054.4-0321	10 56 59.524	-03 37 28.40	0.826	OV96	0.13
MS1137.5+6625	11 40 23.860	66 08 19.15	0.782	HC97	0.15
Abell 1351	11 42 24.592	58 32 06.47	0.32	HC97	0.17
Abell 1413	11 55 18.240	23 24 28.57	0.143	HC97	0.17
Abell 1576	12 36 59.324	63 11 10.31	0.279	OV95	0.21
Abell 1682	13 06 57.220	46 32 41.77	0.226	HC97	0.17
Abell 1689	13 11 30.288	-01 20 25.59	0.180	OV95,HC97	0.23,0.28
Abell 1703	13 15 05.265	51 49 01.88	0.258	OV96	0.40
Abell 1722	13 18 38.372	70 20 20.84	0.327	OV96	0.15
Abell 1763	13 35 20.213	41 00 04.05	0.187	OV95	0.57
MS1358.4+6245	13 59 50.563	62 31 05.34	0.328	OV96	0.22
Abell 1835	14 01 02.021	02 52 41.53	0.252	OV95	0.23
Abell 1914	14 26 02.145	37 50 05.78	0.171	HC96,HC97	0.61,0.44
Abell 1995	14 52 57.564	58 02 55.52	0.318	OV96	0.11
MS1455.0+2232	14 57 15.091	22 20 34.25	0.258	OV96	0.18
RXJ1532+3021	15 32 54.197	30 21 10.79	0.164	HC97	0.11
Abell 2146	15 56 14.375	66 20 56.18	0.233	OV96	0.16
Abell 2163	16 15 46.052	-06 08 55.01	0.208	OV96,HC97	0.21,0.37
Abell 2204	16 32 46.873	05 34 32.32	0.152	HC96	0.32

TABLE 1. (continued)

Cluster Name	RA (J2000.0)	Dec (J2000.0)	Redshift	Obs. Location	$S_{rms}$
Abell 2111	15 39 41.783	34 25 01.02	0.229	HC97	0.15
Abell 2218	16 35 49.486	66 12 44.35	0.171	OV95,HC97	0.13,0.11
Abell 2219	16 40 20.665	46 42 39.78	0.228	OV95	0.26
RXJ1716+6708	17 16 49.138	67 08 23.45	0.813	HC97	0.40
Abell 2259	17 20 09.658	27 40 08.38	0.164	HC96,HC97	0.45,0.28
Abell 2261	17 22 27.073	32 07 58.57	0.224	OV95	0.19
Abell 2294	17 23 55.106	85 53 23.86	0.178	HC97	0.31
RXJ1720+2638	17 20 08.889	26 38 05.96	0.164	HC97	0.37
MS2053.7-0449	20 56 21.771	-04 37 51.46	0.583	OV96	0.40
Abell 2345	21 27 13.635	-12 09 45.41	0.176	OV96	0.54
RXJ2129+0005	21 29 37.887	00 05 38.61	0.235	HC97	0.19
Abell 2409	22 00 54.495	20 57 32.59	0.147	HC97	0.14
Abell 2507	22 56 51.597	05 30 12.20	0.196	OV96	0.19
Abell 2631	23 37 39.738	00 17 36.92	0.27	OV96	0.15

References for Table 1.

HC97 - BIMA June 15 to August 15, 1997; HC96 - BIMA September 1 to 30, 1996; OV96 - OVRO July 15 to September 1, 1996; OV95 - July 1 to August 30, 1995.

TABLE 2. BIMA 1997 1 cm  
calibrator list

J2000.0 Name <sup>a</sup>	1 cm flux (Jy)
0010+109	1.06
0010+174	0.55
0042+233	0.38
0125-000	1.54
0224+069	0.82
0238+166	1.73
0532+075	1.38
0841+708	2.30
0854+201	2.03
0920+446	1.41
0921+622	1.00
0927+390	10.45
1048+717	1.35
1159+292	1.08
1224+035	0.86
1310+323	2.05
1549+026	4.93
1602+334	0.85
1613+342	3.95
1635+381	2.47
1642+398	6.22
1745+173	0.65
1800+784	2.12
1806+698	1.61
2136+006	4.41
2203+315	2.98

<sup>a</sup>J2000.0 name is from the VLA list  
of calibrators.

TABLE 3. Radio Sources at 1 cm and Spectral Indices

Cluster	Name <sup>a</sup>	RA <sup>b</sup>	Dec <sup>b</sup>	S <sub>1cm</sub> (mJy) <sup>c</sup>	S <sub>2cm</sub> (mJy)	S <sub>6cm</sub> (mJy)	S <sub>20cm</sub> (mJy)	$\alpha$	Id	Notes
A68	0037+0907	00 37 06.3	09 07 35	2.45 $\pm$ 0.43			41.9 $\pm$ 1.7 <sup>1</sup>	0.94 $\pm$ 0.11		
	0037+0908	00 37 07.1	09 08 40	1.73 $\pm$ 0.63			51.3 $\pm$ 1.9 <sup>1</sup>	1.12 $\pm$ 0.21		
A267	0152+0102	01 52 54.5	01 02 05	8.84 $\pm$ 1.18			4.7 $\pm$ 0.5 <sup>1</sup>	-0.21 $\pm$ 0.13		Inverted
	0152+0059	01 52 29.8	00 59 34	3.01 $\pm$ 0.88			30.6 $\pm$ 1.1 <sup>1</sup>	0.76 $\pm$ 0.22		
A348	0223-0834	02 23 58.9	-08 34 25	0.68 $\pm$ 0.21						
A370	0237-0147	02 39 55.7	-01 34 31	0.73 $\pm$ 0.24						
A383	0248-0331	02 48 04.1	-03 31 20	4.27 $\pm$ 0.19						
MS0302	0305+1710	03 05 31.6	17 10 04	1.53 $\pm$ 0.40		3.3 <sup>2</sup>		0.43 $\pm$ 0.31		CG
	0305+1711	03 05 27.9	17 11 31	1.12 $\pm$ 0.46						CG
RXJ0439	0439+0715	04 39 01.4	07 15 45	1.14 $\pm$ 0.48			31.8 $\pm$ 1.5 <sup>1</sup>	1.17 $\pm$ 0.32		CG
	0439+0714	04 39 12.2	07 14 11	1.26 $\pm$ 0.39						
A520	0454+0257	04 54 01.1	02 57 46	4.92 $\pm$ 0.95			6.7 $\pm$ 0.5 <sup>1</sup>	0.10 $\pm$ 0.08		
	0454+0255A	04 54 17.2	02 55 33	0.98 $\pm$ 0.21			15.3 $\pm$ 1.1 <sup>1</sup>	0.91 $\pm$ 0.09		
	0455+0255B	04 54 21.1	02 55 02	1.25 $\pm$ 0.24			27.8 $\pm$ 1.6 <sup>1</sup>	1.02 $\pm$ 0.09		
MS0452	0454-0301	04 54 24.3	-03 01 16	1.16 $\pm$ 0.11						
A586	0732+3142	07 32 21.3	31 42 12	2.36 $\pm$ 0.48						
A665	0831+6552	08 31 30.9	65 52 37	5.89 $\pm$ 1.14	12.7 $\pm$ 0.3 <sup>11</sup>	25.7 $\pm$ 1.6 <sup>11</sup>	30.6 $\pm$ 0.3 <sup>11</sup>	0.37 $\pm$ 0.06		
	0830+6550	08 30 26.4	65 50 36	0.66 $\pm$ 0.15	1.1 $\pm$ 0.3 <sup>11</sup>	3.69 $\pm$ 0.14 <sup>11</sup>	12.0 $\pm$ 0.3 <sup>11</sup>	0.78 $\pm$ 0.08		
Zw1953	0850+3604	08 50 08.1	36 04 22	1.67 $\pm$ 0.38			21.9 $\pm$ 1.5 <sup>1</sup>	0.86 $\pm$ 0.18		
Zw2089	0900+2053	09 00 36.5	20 53 41	1.33 $\pm$ 0.49			9.6 $\pm$ 0.5 <sup>1</sup>	0.66 $\pm$ 0.28		
A781	0920+3029	09 20 23.2	30 29 43	6.89 $\pm$ 0.67			74.1 $\pm$ 2.7 <sup>1</sup>	0.78 $\pm$ 0.08		
A851	0942+4658	09 42 57.2	46 58 48	1.35 $\pm$ 0.42			3.1 <sup>3</sup>	0.27 $\pm$ 0.21		
Zw2701	0952+5151	09 52 44.5	51 51 18	18.11 $\pm$ 2.80			3.5 $\pm$ 0.7 <sup>1</sup>	-0.55 $\pm$ 0.19		Inverted
A959	1017+5934	10 17 34.2	59 34 31	0.82 $\pm$ 0.21			15.3 $\pm$ 1.1 <sup>1</sup>	0.97 $\pm$ 0.15		
Zw3146	1023+0409A	10 23 45.1	04 10 40	5.14 $\pm$ 1.10		41 $\pm$ 11 <sup>4</sup>	96.6 $\pm$ 3.5 <sup>1</sup>	0.74 $\pm$ 0.11		
	1023+0409B	10 23 37.2	04 09 06	2.21 $\pm$ 0.36			31.9 $\pm$ 1.0 <sup>1</sup>	0.88 $\pm$ 0.10		
MS1054	1056-0337A	10 56 59.6	-03 37 30	0.64 $\pm$ 0.33		6.1 <sup>2</sup>		1.29 $\pm$ 0.26		CG
	1056-0337B	10 56 48.6	-03 37 33	0.57 $\pm$ 0.34						
A1351	1142+5832	11 42 23.6	58 32 06	6.72 $\pm$ 1.29		41 $\pm$ 6 <sup>4</sup>	104.6 $\pm$ 3.7 <sup>1</sup>	0.77 $\pm$ 0.08		CG (8C 1139+588)
	1142+5831	11 42 19.2	58 31 03	1.15 $\pm$ 0.45			52.6 $\pm$ 3.7 <sup>1</sup>	1.26 $\pm$ 0.22		
A1413	1155+2326	11 55 09.2	23 26 19	2.35 $\pm$ 0.54	1.58 <sup>14</sup>			-0.61 $\pm$ 0.31		Inverted, 0.9 mJy (8.4 GHz) <sup>14</sup>
A1576	1236+6311	12 36 57.4	63 11 16	0.96 $\pm$ 0.21			19.8 $\pm$ 1.0 <sup>1</sup>	1.00 $\pm$ 0.12		
	1234+6328	12 34 19.1	63 28 27	5.51 $\pm$ 0.15			66.4 $\pm$ 2.0 <sup>1</sup>	0.82 $\pm$ 0.05		8C 1234+634
A1682	1306+4633	13 06 45.5	46 33 29	7.76 $\pm$ 1.10		64 $\pm$ 9 <sup>4</sup>	509 $\pm$ 15 <sup>5</sup>	1.02 $\pm$ 0.09		B3 1304+468
A1689	1311-0120	13 11 30.6	-01 20 27	1.31 $\pm$ 0.43		2.75 <sup>7</sup>	10.4 <sup>7</sup>	1.06 $\pm$ 0.12		
	1311-0119	13 11 31.0	-01 19 35	0.52 $\pm$ 0.26		10.7 <sup>7</sup>	41.1 <sup>7</sup>	1.44 $\pm$ 0.14		
A1703	1315+5148	13 15 08.2	51 48 43	1.77 $\pm$ 0.40			47.2 $\pm$ 2.1 <sup>1</sup>	1.09 $\pm$ 0.17		
A1722	1318+7018	13 18 51.7	70 18 45	0.73 $\pm$ 0.25				2.00 $\pm$ 0.31		
A1763	1335+4100	13 35 20.5	41 00 05	27.42 $\pm$ 1.57		24 $\pm$ 4 <sup>6</sup>	858 $\pm$ 30 <sup>1</sup>	1.15 $\pm$ 0.02		CG (4C +41.26)
MS1358	1359+6231	13 59 50.6	62 31 03	1.35 $\pm$ 0.38		224 $\pm$ 27 <sup>4</sup>		0.59 $\pm$ 0.28		2.98 $\pm$ 0.06 Jy (408 MHz) <sup>13</sup>
A1835	1401+0252	14 01 02.2	02 52 43	3.31 $\pm$ 0.94		3.8 <sup>2</sup>	41.4 $\pm$ 1.9 <sup>1</sup>	0.84 $\pm$ 0.21		CG
	1358+0306	13 58 35.3	03 06 10	1.92 $\pm$ 0.74						
A1995	1453+5803	14 53 00.4	58 03 11	0.37 $\pm$ 0.14			8.9 $\pm$ 0.9 <sup>1</sup>	1.05 $\pm$ 0.23		
	1452+5801	14 52 46.9	58 01 48	0.75 $\pm$ 0.16			5.4 $\pm$ 0.5 <sup>1</sup>	0.65 $\pm$ 0.13		

TABLE 3. (continued)

Cluster	Name <sup>a</sup>	RA <sup>b</sup>	Dec <sup>b</sup>	S <sub>1cm</sub> (mJy) <sup>c</sup>	S <sub>2cm</sub> (mJy)	S <sub>6cm</sub> (mJy)	S <sub>20cm</sub> (mJy)	$\alpha$	Id	Notes
MS1455	1457+2220A	14 57 14.9	22 20 34	0.67 $\pm$ 0.32		1.9 <sup>2</sup>		0.59 $\pm$ 0.25	CG	
RXJ1532	1532+3019	15 32 50.6	30 19 48	5.45 $\pm$ 1.26			8.0 $\pm$ 0.5 <sup>1</sup>	0.12 $\pm$ 0.14		
	1532+3020	15 32 53.8	30 20 59	2.49 $\pm$ 0.73			23.3 $\pm$ 0.8 <sup>1</sup>	0.74 $\pm$ 0.17		
A2146	1556+6620	15 56 13.9	66 20 53	2.16 $\pm$ 0.59			15.8 $\pm$ 0.6 <sup>1</sup>	0.66 $\pm$ 0.16	CG	
	1556+6622	15 56 04.1	66 22 15	2.02 $\pm$ 0.77			42.5 $\pm$ 1.7 <sup>1</sup>	1.01 $\pm$ 0.22		
A2163	1615-0608	16 15 43.6	-06 08 45	1.12 $\pm$ 0.29	3 <sup>15</sup>	2 <sup>15</sup>				Unusual spectrum
A2204	1632+0534	16 32 46.8	05 34 32	6.77 $\pm$ 1.25				0.85 $\pm$ 0.16	CG (TXS 1630+056)	275 $\pm$ 20 mJy (365 MHz) <sup>10</sup>
	1632+0531	16 32 42.5	05 31 46	4.10 $\pm$ 0.85		51 $\pm$ 11 <sup>8</sup>		1.42 $\pm$ 0.30	PMNJ1632+0531	
A2218	1635+6613	16 35 22.0	66 13 19	3.08 $\pm$ 0.25	4.99 $\pm$ 0.60 <sup>11</sup>	2.82 $\pm$ 0.15 <sup>11</sup>	1.25 $\pm$ 0.21 <sup>11</sup>			Unusual spectrum
	1635+6614	16 35 47.4	66 14 42	0.91 $\pm$ 0.17	2.36 $\pm$ 0.62 <sup>11</sup>	3.66 $\pm$ 0.25 <sup>11</sup>	8.12 $\pm$ 0.46 <sup>11</sup>	0.66 $\pm$ 0.05	5C20.92/94	
	1636+6614	16 36 15.7	66 14 21	1.05 $\pm$ 0.14	2.01 $\pm$ 0.52 <sup>11</sup>	4.21 $\pm$ 0.13 <sup>11</sup>	7.61 $\pm$ 0.21 <sup>11</sup>	0.57 $\pm$ 0.02	5C20.101	
A2219	1640+4642	16 40 21.9	46 42 46	17.44 $\pm$ 1.66		81 $\pm$ 10 <sup>4</sup>	240 $\pm$ 8.4 <sup>1</sup>	0.87 $\pm$ 0.08	CG (B3 1638+468)	710 $\pm$ 20 mJy (408 MHz) <sup>13</sup>
RXJ1716	1716+6708	17 16 36.5	67 08 28	3.41 $\pm$ 0.52		87 $\pm$ 6 <sup>4</sup>	335 $\pm$ 11.5 <sup>10</sup>	1.09 $\pm$ 0.11	4C +67.26	
A2261	1722+3209	17 22 18.9	32 09 18	3.88 $\pm$ 0.88			10.0 $\pm$ 2 <sup>9</sup>	0.31 $\pm$ 0.11		
A2345	2127-1210	21 27 12.9	-12 09 45	6.02 $\pm$ 1.74			265 $\pm$ 9.2 <sup>1</sup>	1.17 $\pm$ 0.10	CG (MRC 2124-123)	890 $\pm$ 70 mJy (408 MHz) <sup>12</sup>
RXJ2129	2129+0005	21 29 40.1	00 05 26	1.89 $\pm$ 0.43			26.2 $\pm$ 1.2 <sup>1</sup>	0.87 $\pm$ 0.13		
	2129+0007	21 29 56.1	00 07 57	0.61 $\pm$ 0.21			36.9 $\pm$ 2.0 <sup>1</sup>	1.36 $\pm$ 0.23		
A2409	2201+2054	22 01 10.2	20 55 04	3.38 $\pm$ 0.65			4.3 $\pm$ 0.4 <sup>1</sup>	0.08 $\pm$ 0.12		
A2507	2256+0531	22 56 43.8	05 31 15	6.42 $\pm$ 1.89			14.8 $\pm$ 0.61 <sup>1</sup>	0.28 $\pm$ 0.17		
A2631	2237+0016	22 37 40.4	00 16 46	3.87 $\pm$ 0.76			107.9 $\pm$ 3.8 <sup>1</sup>	1.10 $\pm$ 0.11		

<sup>a</sup>J2000.0 Name<sup>b</sup>Source position of the observed 1 cm sources (J2000.0).<sup>c</sup>Corrected 1 cm flux densities of the detected radio sources.

References for Table 3.

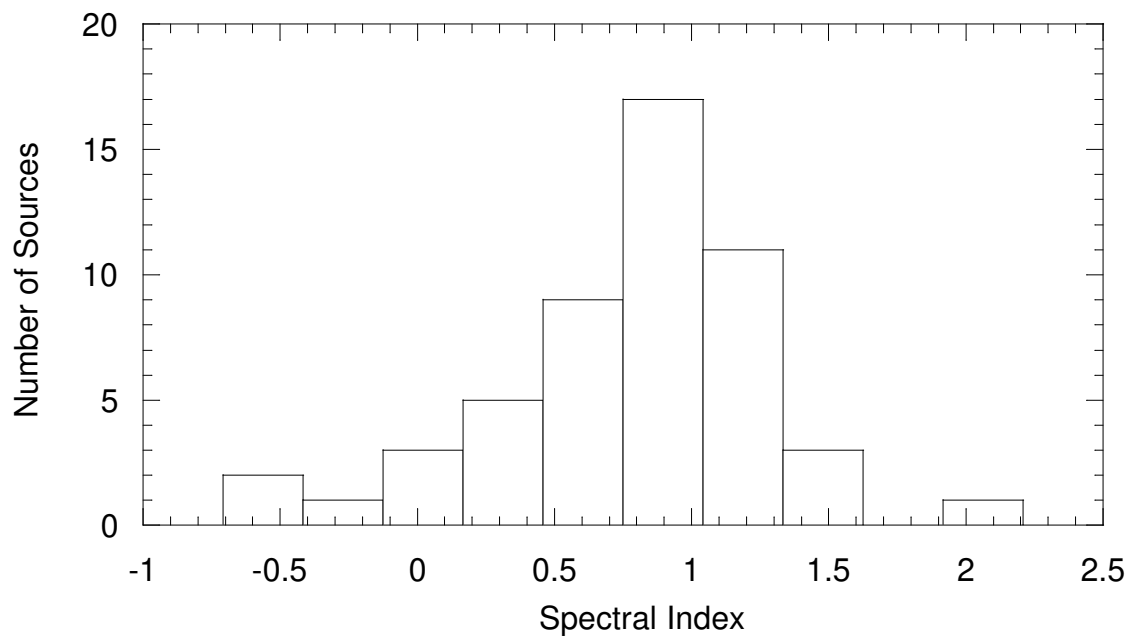
(1) NVSS Survey, Condon *et al.* (1996); (2) Gioia & Luppino 1994; (3) Condon, Dickey & Salpeter 1990; (4) 87GB, Gregory & Condon 1991; (5) White & Becker 1992; (6) Becker, White & Edwards 1991; (7) Slee *et al.* 1994; (8) Griffith *et al.* 1995; (9) FIRST Survey, Becker *et al.* 1995; (10) Douglas *et al.* 1996; (11) Moffet & Birkinshaw 1989; (12) Robertson & Roach 1990; (13) Ficarra *et al.* 1985; (14) Grainge *et al.* 1996; (15) Herbig & Birkinshaw 1994.

TABLE 4. 1 cm counterparts of MB sources

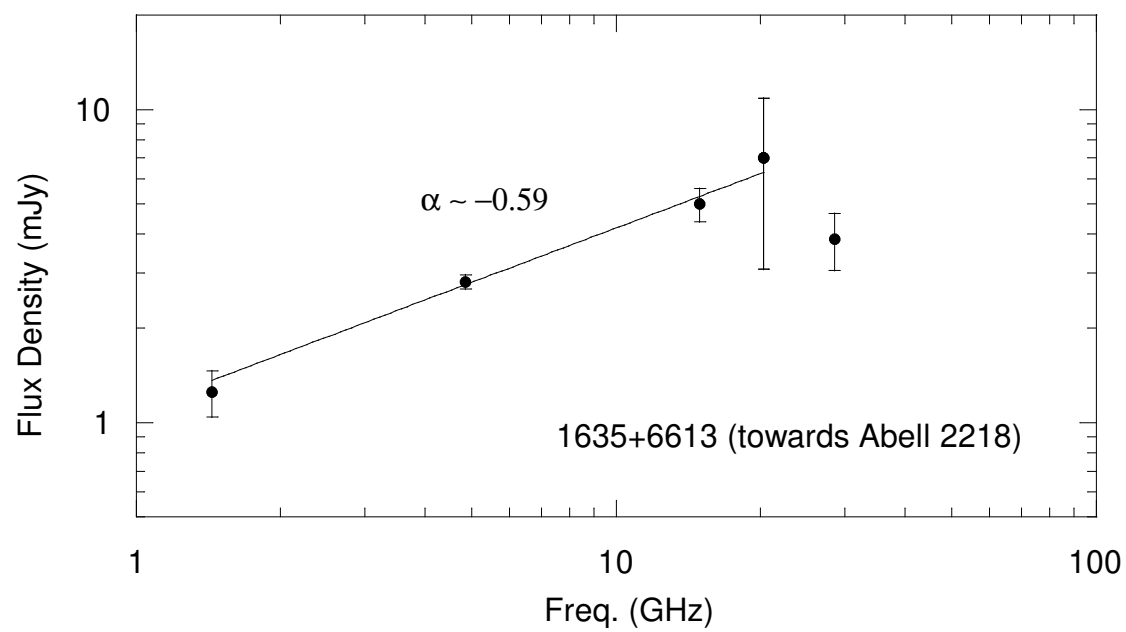
Cluster Name	MB Source Number	$S_{1.4\text{GHz}}$ (mJy)	$S_{28.5\text{GHz}}^{exp}$ (mJy)	$S_{28.5\text{GHz}}^{obs}$ (mJy)	$\alpha$
CL0016+16	14	$2.69 \pm 0.69$	$< 2$	$< 0.20$	$> 0.86$
	15	$267 \pm 3$	15.8	$10.11 \pm 1.11$	$0.96 \pm 0.07$
Abell 665	12	$12 \pm 0.3$	0.7	$0.66 \pm 0.15$	$0.96 \pm 0.09$
	17	$7.06 \pm 0.46$	$< 1.3$	$0.50 \pm 0.32$	$0.77 \pm 0.10$
	20	$30.6 \pm 0.3$	19.9	$5.98 \pm 1.14$	$0.37 \pm 0.06$
	21	$2.34 \pm 0.20$	0.4	$0.44 \pm 0.21$	$0.58 \pm 0.18$
Abell 2218	12	$1.25 \pm 0.21$	9.2	$3.08 \pm 0.25$	$0.29 \pm 0.06$
	15	$2.37 \pm 0.21$	0.1	$< 0.29$	$> 0.90$
	16	$8.12 \pm 0.46$	1.1	$0.91 \pm 0.17$	$0.66 \pm 0.05$
	17	$2.79 \pm 0.09$	$< 0.05$	$< 0.18$	$> 0.91$
	21	$7.61 \pm 0.21$	1.8	$1.05 \pm 0.14$	$0.57 \pm 0.02$

References for Table 4.

MB - Moffet & Birkinshaw (1989)

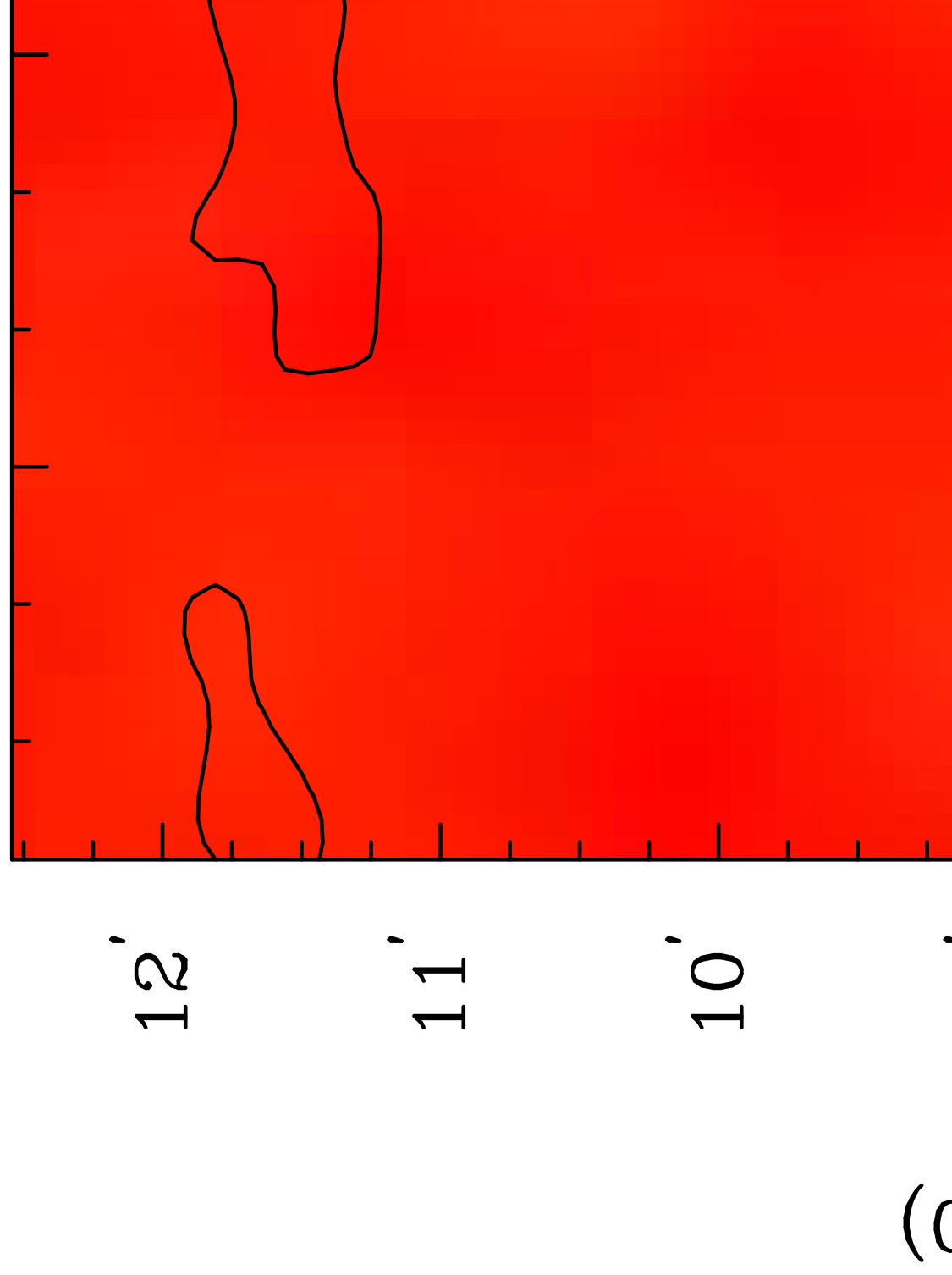




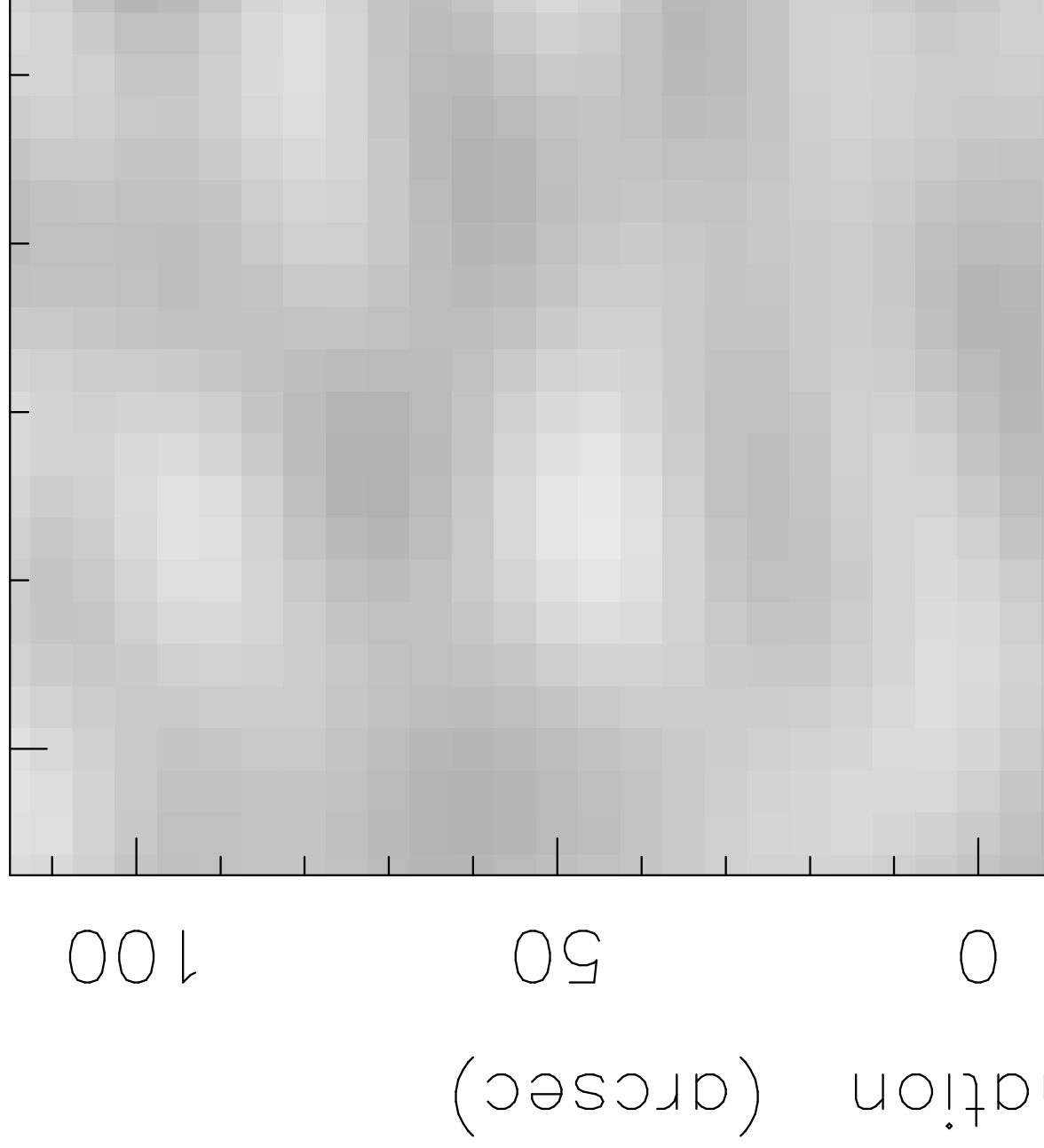




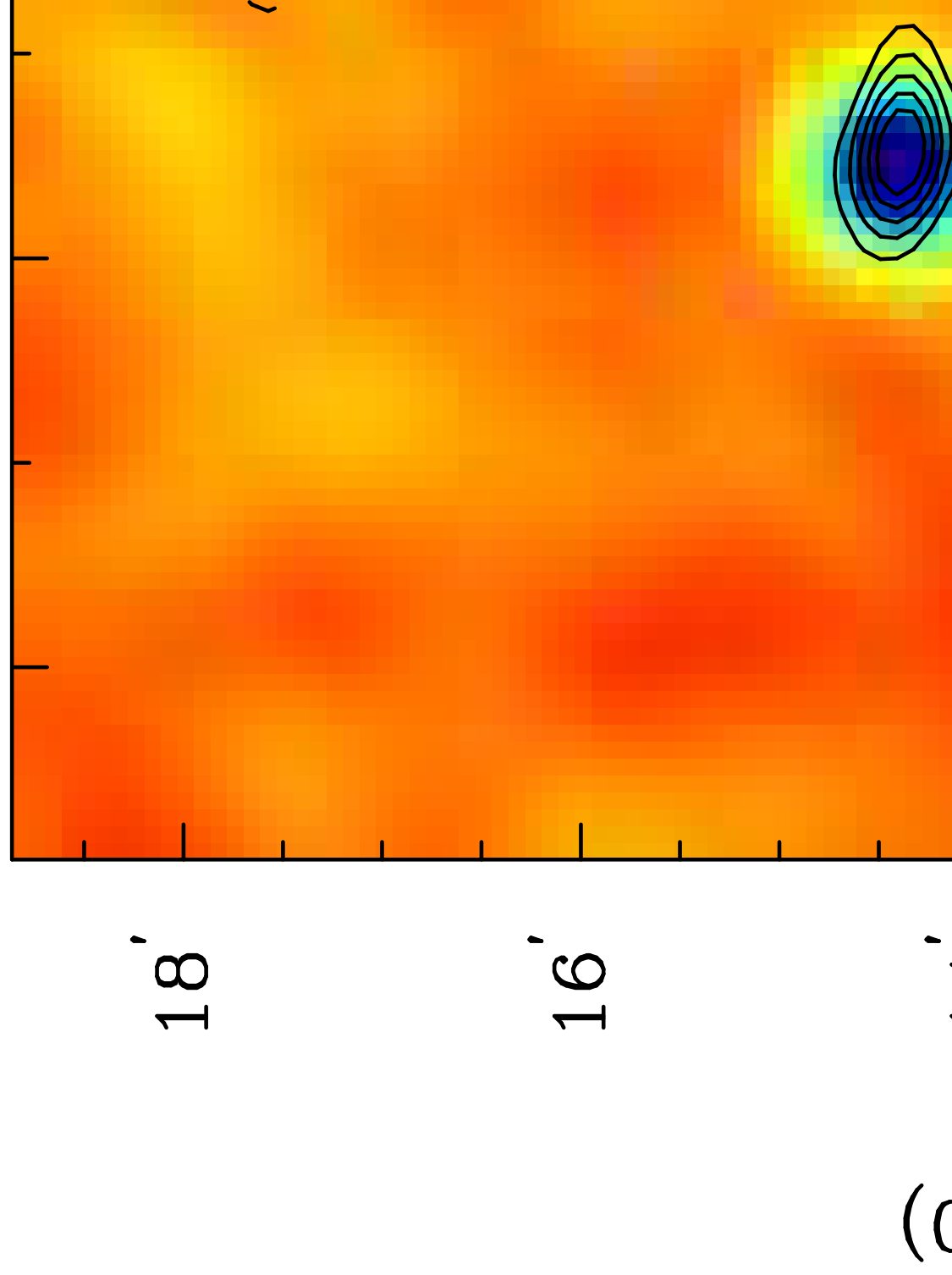
Abell 68: BIMA 1997 28.5

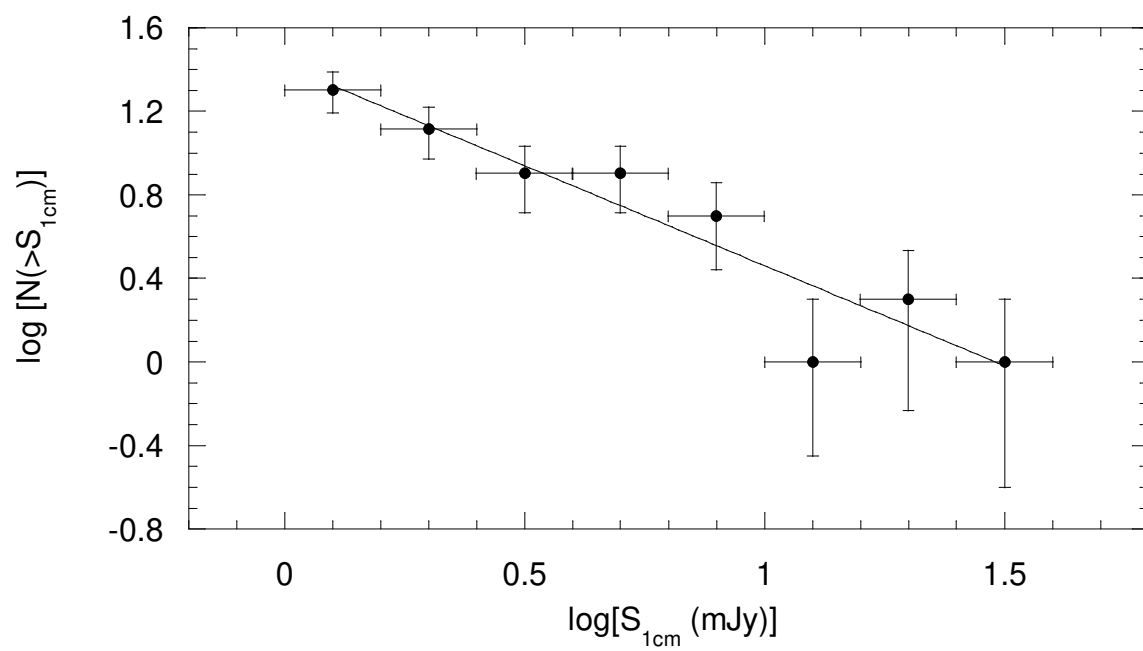


Clean map. Array: r  
RXJ1716+ at 28.503



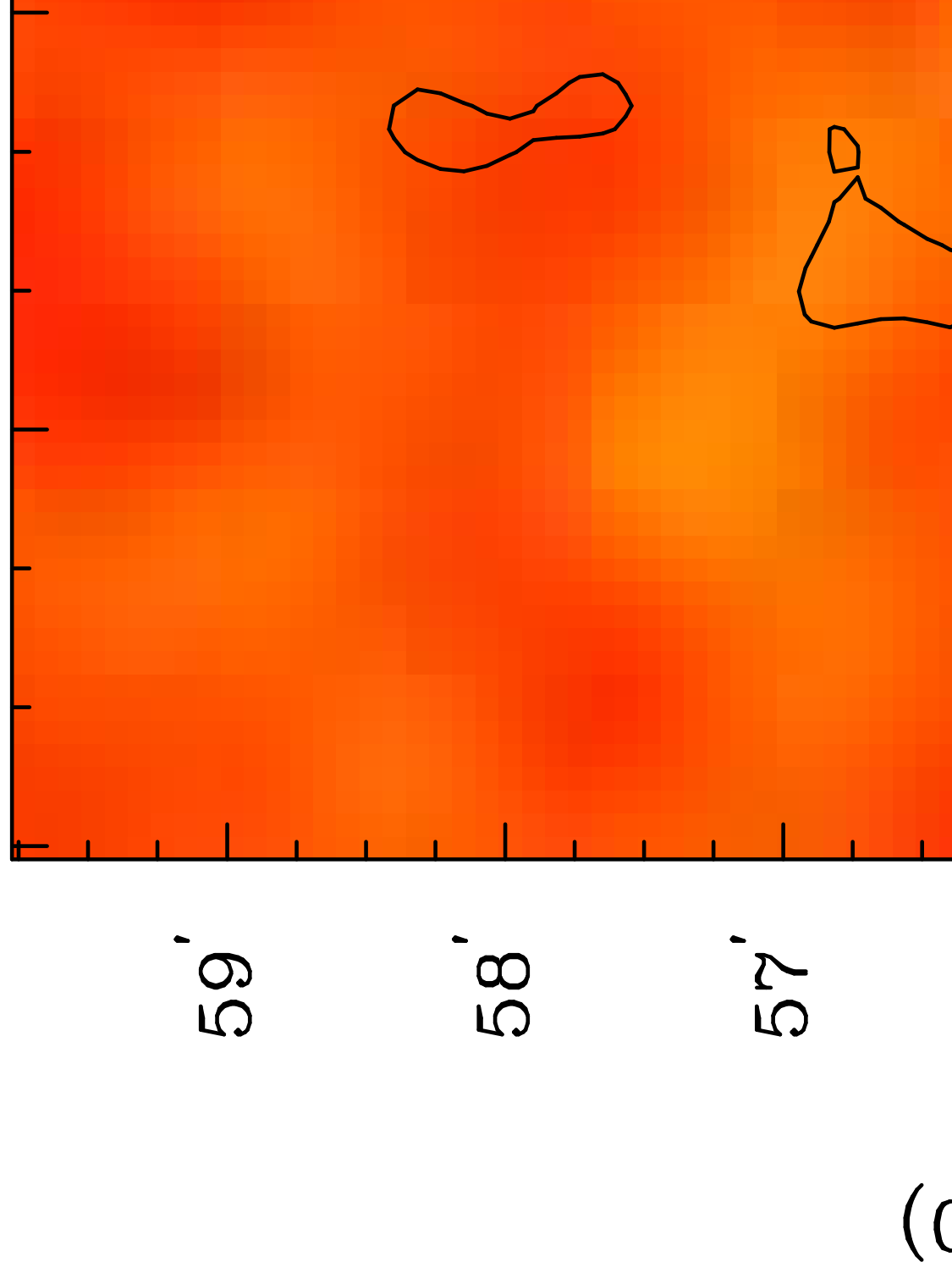
Abell 2218: BIMA 1997 28.



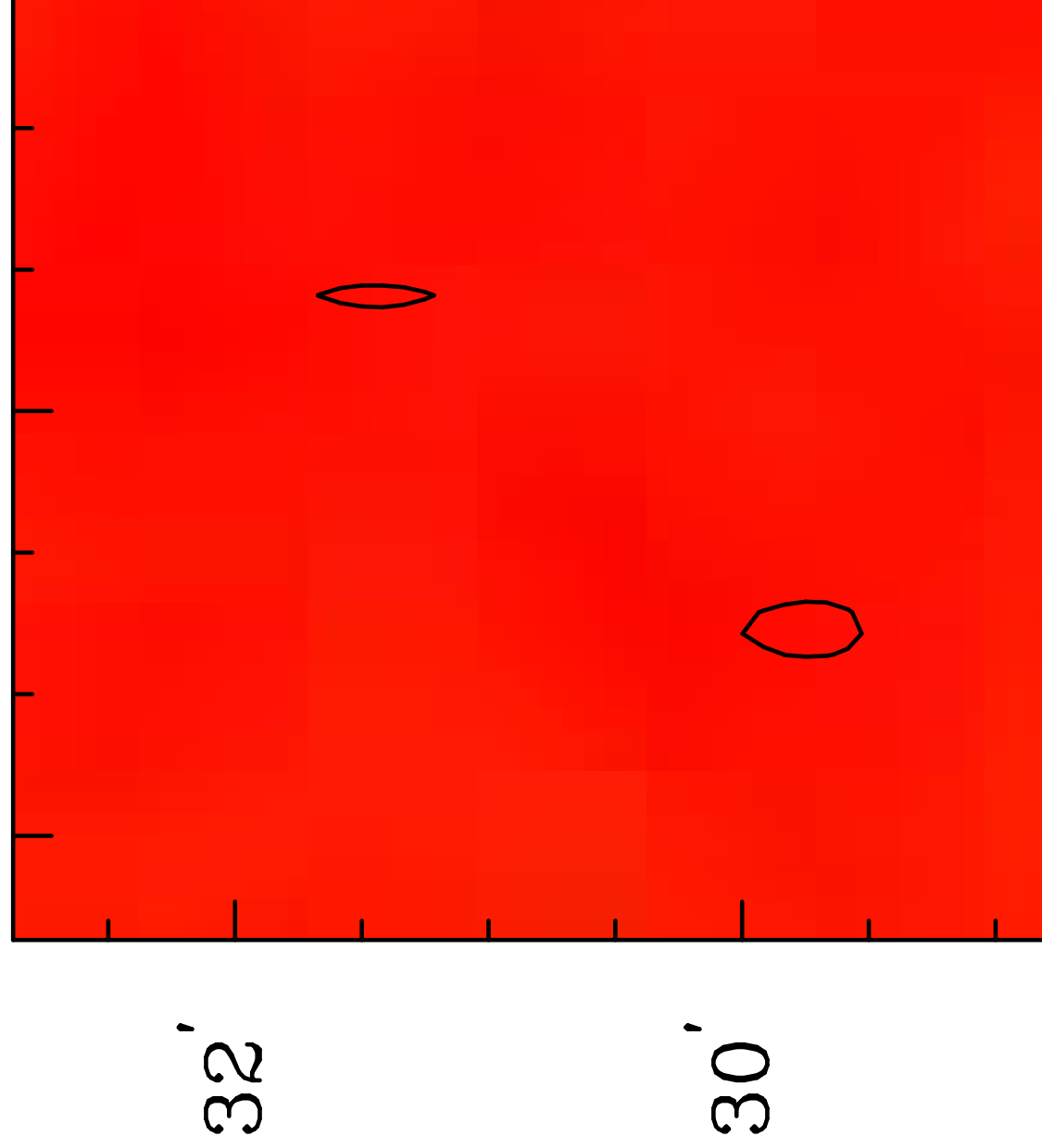




Abell 520: BIMA 1997 28.5



Abell 1576: OVR0 1996 30



32'

30'

(c)